

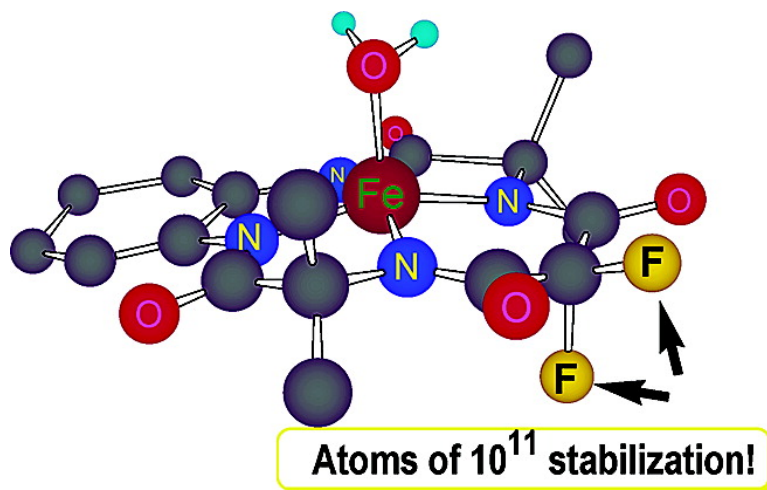
Communication

Understanding the Mechanism of H-Induced Demetalation as a Design Strategy for Robust Iron(III) Peroxide-Activating Catalysts

Anindya Ghosh, Alexander D. Ryabov, Sherry M. Mayer, David C. Horner, Duane E. Prasuhn, Sayam Sen Gupta, Leonard Vuocolo, Caleb Culver, Michael P. Hendrich, Clifton E. F. Rickard, Richard E. Norman, Colin P. Horwitz, and Terrence J. Collins

J. Am. Chem. Soc., **2003**, 125 (41), 12378-12379 • DOI: 10.1021/ja0367344 • Publication Date (Web): 19 September 2003

Downloaded from <http://pubs.acs.org> on March 29, 2009



More About This Article

Additional resources and features associated with this article are available within the HTML version:

- Supporting Information
- Links to the 4 articles that cite this article, as of the time of this article download
- Access to high resolution figures
- Links to articles and content related to this article
- Copyright permission to reproduce figures and/or text from this article

[View the Full Text HTML](#)

Understanding the Mechanism of H⁺-Induced Demetalation as a Design Strategy for Robust Iron(III) Peroxide-Activating Catalysts

Anindya Ghosh,[†] Alexander D. Ryabov,[†] Sherry M. Mayer,[†] David C. Horner,[†] Duane E. Prasuhn, Jr.,[†] Sayam Sen Gupta,[†] Leonard Vuocolo,[‡] Caleb Culver,[†] Michael P. Hendrich,^{*,†} Clifton E. F. Rickard,[§] Richard E. Norman,^{||} Colin P. Horwitz,[†] and Terrence J. Collins^{*,†}

Department of Chemistry, Carnegie Mellon University, 4400 Fifth Avenue, Pittsburgh, Pennsylvania 15213, Department of Chemistry, Allegheny College, Box 15, Meadville, Pennsylvania 16335, Department of Chemistry, University of Auckland, Private Bag 92019, Auckland, New Zealand, and Department of Chemistry, University of Louisiana at Monroe, CNSB-210, Monroe, Louisiana 71209

Received June 17, 2003; E-mail: hendrich@andrew.cmu.edu; tc1u@andrew.cmu.edu

Enzymes that activate dioxygen or hydrogen peroxide exhibit remarkable catalytic activity and selectivity, but oxidative and hydrolytic fragility limit their technological applicability. Their catalytic activity–pH profiles are usually bell-shaped, resulting from either reversible or irreversible activity loss at extreme pH.¹ Their mere existence challenges chemists to design low-molecular, protein-free catalysts² that are at least as active, while being more robust in aggressively oxidizing acidic and basic environments. Recently, we introduced a new class of oxidatively robust “green”³ catalysts for H₂O₂ oxidation of a wide spectrum of substrates⁴ including facile polychlorophenol mineralization.⁵ The Fe^{III} centers of the nontoxic catalysts⁵ are coordinated to tetra-amido macrocyclic ligands giving TAML oxidant activators, Figure 1.

When extracted from the protein environments of horseradish peroxidase (HRP) or cytochrome P450, the catalytic properties of the Fe^{III} porphyrin cofactors are inadequate. In contrast, Fe^{III}-TAML activators are exceptionally active; the second-order rate constants for the rate-limiting activation of H₂O₂ are as high as 10⁴ M⁻¹ s⁻¹ at 25 °C and optimal pH.⁶ TAML catalysts are effective in nanomolar to low micromolar concentrations in water where they can attain turnover frequencies in the thousands per minute.⁵ Despite this high activity, the design protocol applied to developing Fe^{III}-TAML activators (R = alkyl) led, inter alia, to their protection from rapid oxidative degradation. However, as with HRP, they rapidly lose activity at pH < 4 by demetalation, although HRP's Fe^{III}-porphyrin is more resistant to acidic conditions.⁷

Inactivation mechanisms for small molecule TAML activators should be much easier to understand than those of enzymes, and such understanding should facilitate the design of more stable catalysts. We illustrate this argument using structural, spectral, kinetic, and mechanistic studies of Fe^{III}-TAML activators. Stabilization against H⁺-induced demetalation has been achieved of 10⁵-fold and 10¹¹-fold in mildly and strongly acidic solutions, respectively.

Iron(III)-TAML activators are synthesized either in chloro or in aqua forms (Figure 1).⁸ X-ray structures demonstrate 5-coordination (5-CN) with long Fe–Cl (**1a,e**) and Fe–OH₂ (**2a**) bonds (Figure 1 and Supporting Information).⁹ 5-CN is typical of HRP iron.^{1b} If the same geometry holds in solution, the open axial site could contribute to both high catalytic activity of Fe^{III}-TAMLS toward H₂O₂ and the facile proteolysis. The speciation of Fe^{III}-TAMLS in water was studied by UV/vis and EPR. Principal conclusions derived from consistent results (Supporting Information) are summarized below and shown in Scheme 1. (i) The chloro ligands of

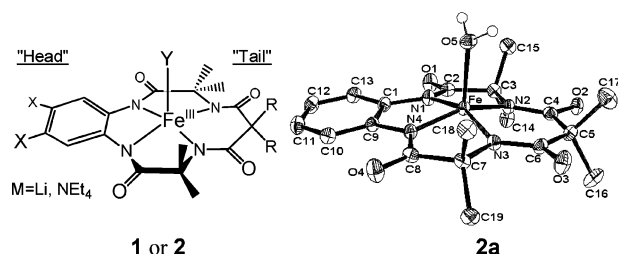
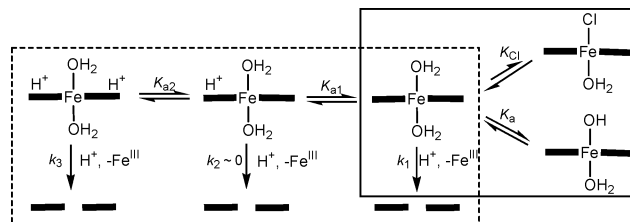


Figure 1. Fe^{III}-TAML activators **1** (Y = Cl) and **2** (Y = H₂O): **a** (R = Me, X = H), **b** (Me, Cl), **c** (Me, MeO), **d** (Et, Cl), **e** (F, H), **f** (F, Cl), and crystal structure of **2a**. Iron is 0.363(1) Å above the 4-N_{av} plane with a long Fe^{III}–O bond of 2.097(2) Å arising from ground-state weakening by the four very strong σ -N-donors. For X-ray structures of **1b** and **1e**, see Supporting Information.

Scheme 1. Speciation of Fe^{III}-TAML Activators in Aqueous Solution (Solid Rectangle) and Suggested Mechanism of the H⁺-Induced Demetalation (Dashed Rectangle); – = Free Base Ligand



1 undergo rapid hydrolysis as expected for species with long Fe–Cl bonds;¹⁰ equilibrium data, K_{Cl} (Table 1), indicate insignificant Cl⁻ coordination for [Cl⁻] ≤ 0.5 M. (ii) Cl⁻ hydrolysis affords aqua species accounting for the similarity of **1** and **2** UV/vis and EPR spectra in water. (iii) The aqua species are 6-CN in water. (iv) UV/vis and EPR spectra are independent of pH from 5 to 8, but vary reversibly at 8–11 with deprotonation of an aqua ligand; for **2b**, a band at 368 nm disappears with increasing pH (isosbestic point at 345 nm). pK_a 's are in the range 9.4–10.5 (Table 1).

Aqueous solutions of **2** (R = Me) at neutral pH are stable for months, but at pH 3–4 the UV/vis band around 360 nm fades irreversibly. The free macrocyclic ligand was isolated in >95% yield treating **2a** at pH 1. For this reaction, the plot of the pseudo-first-order rate constants, k_{obs} , versus the concentration of HClO₄ or HCl is distinctly curved, indicating high-order pathways in [H⁺] (Figure 2). Best fits were obtained using $k_{obs} = k_1[H^+] + k_3[H^+]^3$. Adding a second-order term $k_2[H^+]^2$ did not improve the fit for any complex. General acid catalysis is minor, because k_{obs} is virtually identical in 0.01 and 0.1 M phosphate at pH 4. The k_1 * pathway is 3 times faster in D⁺/D₂O than in H⁺/H₂O, $k_H/k_D =$

[†] Carnegie Mellon University.

[‡] Allegheny College.

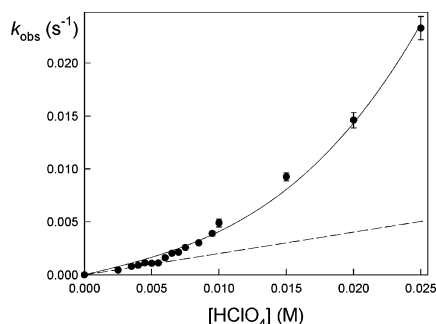
[§] University of Auckland.

^{||} University of Louisiana at Monroe.

Table 1. Equilibrium and Kinetic Parameters for Fe-TAMLs at 25 °C

2	pK _a	K _{C1} (M ⁻¹) ^a	k ₁ [*] (M ⁻¹ s ⁻¹) ^b	k ₃ [*] (M ⁻³ s ⁻¹) ^b
2a	10.1 ± 0.6	0.18 ± 0.04	2.2 ± 0.7 6.1 ± 0.5 ^c	(6.7 ± 0.2) × 10 ⁵ (6.4 ± 0.3) × 10 ⁵ a
2b	10.0 ± 0.2	0.21 ± 0.09	5.19 ± 0.06	(1.13 ± 0.01) × 10 ⁶
2c	10.5 ± 0.5	>0.05	7.1 ± 0.5	(6.7 ± 0.5) × 10 ⁵
2d	10.4 ± 0.3		0.31 ± 0.02	(1.03 ± 0.05) × 10 ³
2e	9.5 ± 0.4	1.9 ± 0.2	(1.6 ± 0.1) × 10 ⁻⁴	(1.6 ± 0.2) × 10 ⁻⁴
2f	9.4 ± 0.6	2.4 ± 0.4	(3.7 ± 0.4) × 10 ⁻⁵	(4.8 ± 0.6) × 10 ⁻⁵

^a pH 7. ^b 0.1 M KPF₆. ^c In DCl/D₂O.

**Figure 2.** Dependence of k_{obs} versus $[\text{H}^+]$ for **2d** demetalation; 25 °C, 0.1 M KPF₆. The solid line is calculated using the best-fit k_1^* , k_3^* values. The broken line shows the first-order pathway dominating at lower $[\text{HClO}_4]$.

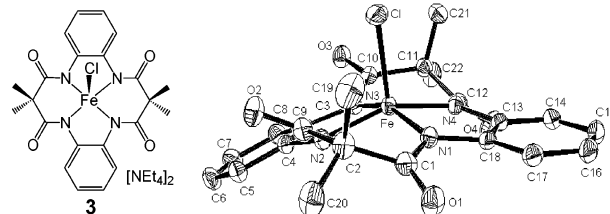
0.36 for **2a**. This reverse isotope effect indicates that a stronger bond is formed in the rate-determining process.¹¹ This suggests that the rate-limiting event for the k_1^* pathway could involve protonation of an amido-nitrogen or an N–Fe bond, forming the N–H bond as the weaker N–Fe bond is cleaved. $k_{\text{H}}/k_{\text{D}} \approx 1$ for the k_3^* pathway, making it more difficult to suggest mechanistic details for this pathway; preequilibrium peripheral protonations of the macrocycle are likely steps (Scheme 1). The dependence of k_{obs} on $[\text{H}^+]$ is given by eq 1, which corresponds to the experimental rate law when equilibrium constants K_{a1} and K_{a2} are high (i.e., **2** complexes are weak bases), ensuring $K_{a1}K_{a2} \gg (K_{a2}[\text{H}^+] + [\text{H}^+]^2)$ and k_2 is negligible as compared to k_1 and k_3 , that is, $(k_1K_{a1}K_{a2}[\text{H}^+] + k_3[\text{H}^+]^3) \gg k_2K_{a2}[\text{H}^+]^2$, with $k_1^* = k_1$ and $k_3^* = k_3(K_{a1}K_{a2})^{-1}$.

$$k_{\text{obs}} = \frac{(k_1K_{a1}K_{a2}[\text{H}^+] + k_2K_{a2}[\text{H}^+]^2 + k_3[\text{H}^+]^3)}{(K_{a1}K_{a2} + K_{a2}[\text{H}^+] + [\text{H}^+]^2)} \quad (1)$$

The rate of acid-induced demetalation depends only slightly on the nature of the head substituents X (Table 1). In contrast, the tail-R groups dramatically affect k_1^* and, for the most part, k_3^* , suggesting that tail amide O-atoms are sites of peripheral protonation. This suggested a strategy for producing acid tolerant Fe^{III}-TAML catalysts; tail electron-withdrawing groups should reduce the hydrolytic demetalation rate. Replacement of the tail groups R = Me with R = F produces a remarkable stabilization. The rate constants (Table 1) show that under weakly acidic conditions, when the k_1^* pathway dominates over k_3^* , fluorinated **2f** is 10⁵-fold more H⁺-tolerant than **2a**.

Under more acidic conditions when the k_3^* pathway contribution to the overall rate is major, the difference reaches a unique 11 orders of magnitude, suggesting that the preequilibrium protonations involve at least one tail amide oxygen. At a pH of 4.5, **2f** is a highly active bleaching catalyst, whereas **2a** is inactive.

A mechanism with a preequilibrium M–N cleavage is unlikely for **2** because cleavage of a single M–N bond should cause a strong distortion of the planar complex and induce rapid cleavage of the remaining M–N bonds; distorted TAML ligands tend to have nonplanar amides and high hydrolytic instability, for example, **3**

**Figure 3.** X-ray structure of highly distorted TAML complex **3** (see Supporting Information).

(Figure 3).¹² Very rapid hydrolysis of **3** follows the rate law $k_{\text{obs}} (\text{s}^{-1}) = (2 \pm 1) + (5.5 \pm 0.5) \times 10^3 [\text{H}^+]$; **3** is so labile that rapid hydrolysis occurs in water at pH 7. k_1^* for **3** is > 1000 times faster than that for the most reactive complex in Table 1.

In conclusion, the iterative design approach used to develop oxidatively stable TAML activators⁵ has been extended to control acid-induced hydrolysis. TAML activators with tail electron-withdrawing groups are significantly protected. The entire acidic pH range is now available for exploration of oxidation catalysis using TAML activators. This work also shows that one can destroy any TAML activator by acid treatment for a period determined by its known acidolysis rate, prescribing an easy method for postuse catalyst destruction.

Acknowledgment. T.J.C. thanks Eden-Hall Foundation, NSF (9612990), DOE (NETL), and the Institute for Green Oxidation Chemistry for support. A.G. thanks Theresa Heinz for the award of an Environmental Scholarship in her name. S.M.M. and D.C.H. thank Howard Hughes Medical Institute for support. R.E.N. thanks the Kresge Foundation and Louisiana Board of Regents Support Fund. M.P.H. thanks the NIH (49970).

Supporting Information Available: Experimental procedures, EPR, pH titration data, details of the X-ray investigations (CIF and PDF). This material is available free of charge via the Internet at <http://pubs.acs.org>.

References

- (a) Fersht, A. *Structure and mechanism in protein science: a guide to enzyme catalysis and protein folding*; Freeman: New York, 1999. (b) Dunford, H. B. *Heme Peroxidases*; Wiley-VCH: New York, 1999.
- For selected examples of such catalysts, see: (a) Sorokin, A.; Seris, J.-L.; Meunier, B. *Science* **1995**, *268*, 1163. (b) White, M. C.; Doyle, A. G.; Jacobsen, E. N. *J. Am. Chem. Soc.* **2001**, *123*, 7194. (c) Zuwei, X.; Ning, Z.; Yu, S.; Kunlan, L. *Science* **2001**, *292*, 1139. (d) Kamata, K.; Yonehara, K.; Sumida, Y.; Yamaguchi, K.; Hikichi, S.; Mizuno, N. *Science* **2003**, *300*, 964.
- Collins, T. J. *Science* **2001**, *291*, 48.
- (a) Collins, T. J. *Acc. Chem. Res.* **1994**, *27*, 279; (b) **2002**, *35*, 782.
- Sen Gupta, S.; Stadler, M.; Noser, C. A.; Ghosh, A.; Steinhoff, B.; Lenoir, D.; Horwitz, C. P.; Schramm, K.-W. *Science* **2002**, *298*, 326.
- Ryabov, A. D.; Ghosh, A.; Mitchel, D.; Collins, T. J., in preparation.
- (a) Berezin, B. D.; Drobysheva, A. N. *Zh. Fiz. Khim.* **1974**, *48*, 2742. (b) Espenson, J. H.; Christensen, R. J. *Inorg. Chem.* **1977**, *16*, 2561. (c) Hasegawa, E.; Matsubuchi, E.; Tsuchida, E. *Bull. Chem. Soc. Jpn.* **1991**, *64*, 2289.
- Patents of the Collins Group including key experimental procedures, <http://www.chem.cmu.edu/groups/Collins/awardpatpub/patents/index.html>.
- (a) Bartos, M. J.; Kidwell, C.; Kauffmann, K. E.; Gordon-Wylie, S. W.; Collins, T. J.; Clark, G. C.; Münck, E.; Weintraub, S. T. *Angew. Chem.* **1995**, *107*, 1345; *Angew. Chem., Int. Ed. Engl.* **1995**, *34*, 1216. (b) Bartos, M. J.; Gordon-Wylie, S. W.; Fox, B. G.; Wright, L. J.; Weintraub, S. T.; Kauffmann, K. E.; Münck, E.; Kostka, K. L.; Uffelman, E. S.; Rickard, C. E. F.; Noon, K. R.; Collins, T. J. *Coord. Chem. Rev.* **1998**, *174*, 361.
- (a) Ryabov, A. D.; Kazankov, G. M.; Yatsimirsky, A. K.; Kuz'mina, L. G.; Burtseva, O. Y.; Dvortsova, N. V.; Polyakov, V. A. *Inorg. Chem.* **1992**, *31*, 3083. (b) Schmülling, M.; Ryabov, A. D.; van Eldik, R. J. *Chem. Soc., Dalton Trans.* **1994**, 1257. (c) Schmülling, M.; Grove, D. M.; van Koten, G.; van Eldik, R.; Veldman, N.; Spek, A. L. *Organometallics* **1996**, *15*, 1384.
- (a) Jencks, W. P. *Catalysis in Chemistry and Enzymology*; McGraw-Hill: New York, 1969. (b) Espenson, J. H. *Chemical Kinetics and Reaction Mechanisms*, 2nd ed.; McGraw-Hill: New York, 1995.
- For the synthesis of **3**, see: Sen Gupta, S. PhD Thesis, Department of Chemistry; Carnegie Mellon University: Pittsburgh, PA, 2002; p 137.

JA0367344